Structural, topographical and magnetic evolution of RF-sputtered Fe-Ni alloy based thin films with thermal annealing

2014 Mater. Res. Express 1 015707

(http://iopscience.iop.org/2053-1591/1/1/015707)

Materials Research
Express

Structural, topographical and magnetic evolution of RF-sputtered Fe-Ni alloy based thin films with thermal annealing

R Lisha[1], T Hysen[2], P Geetha[1], D K Avasthi[3], R V Ramanujan[4] and M R Anantharaman[1]

[1] Department of Physics, Cochin University of Science and Technology, Cochin-682022, Kerala, India
[2] Department of Physics, Christian College, Chengannur, Kerala 689 122, India
[3] Inter University Accelerator Centre, Aruna Asaf Ali Marg, New Delhi-110067, India
[4] School of Materials Science and Engineering, Nanyang Technological University, Singapore 639 798
E-mail: mraiyer@gmail.com

Received 12 September 2013, revised 10 January 2014
Accepted for publication 16 January 2014
Published 7 March 2014

Materials Research Express **1** (2014) 015707

doi:10.1088/2053-1591/1/1/015707

Abstract

Metglas 2826 MB having a nominal composition of $Fe_{40}Ni_{38}Mo_4B_{18}$ is an excellent soft magnetic material and finds application in sensors and memory heads. However, the thin-film forms of $Fe_{40}Ni_{38}Mo_4B_{18}$ are seldom studied, although they are important in micro-electro-mechanical systems/nano-electro-mechanical systems devices. The stoichiometry of the film plays a vital role in determining the structural and magnetic properties of $Fe_{40}Ni_{38}Mo_4B_{18}$ thin films: retaining the composition in thin films is a challenge. Thin films of 52 nm thickness were fabricated by RF sputtering technique on silicon substrate from a target of nominal composition of $Fe_{40}Ni_{38}Mo_4B_{18}$. The films were annealed at temperatures of 400 °C and 600 °C. The micro-structural studies of films using glancing x-ray diffractometer (GXRD) and transmission electron microscope (TEM) revealed that pristine films are crystalline with $(FeNiMo)_{23}B_6$ phase. Atomic force microscope (AFM) images were subjected to power spectral density analysis to understand the probable surface evolution mechanism during sputtering and annealing. X-ray photoelectron spectroscopy (XPS) was employed to determine the film composition. The sluggish growth of crystallites with annealing is attributed to the presence of molybdenum in the thin film. The observed changes in magnetic properties were correlated with annealing induced structural, compositional and morphological changes.

Keywords: RF sputtering, crystallite size, coercivity, Metglas, $(FeNiMo)_{23}B_6$ phases

1. Introduction

During the past few decades there has been a tremendous increase in the research, development, and application of soft magnetic materials in various fields, ranging from transformer cores to micro-electro-mechanical systems/nano-electro-mechanical systems devices. Amorphous and nanocrystalline soft magnetic alloys have supplemented and replaced conventional soft magnetic ferrites and Ni-Fe cores in industrial electronics [1]. The magnetic softness of the new class of materials, invented in 1959 by Paul Duwez, is attributed to their biphasic microstructure [2]. Typically, for Fe-based nanocrystalline alloys, the grain size as well as the intergrain separation is about 5–25 nm, which is less than the exchange length (L_{ex}) of these alloys. According to the random anisotropy model (RAM) put forward by Herzer, this is the necessary and sufficient condition for averaging of magnetocrystalline anisotropies over several grains [3]. RAM predicts that the coercivity of nanocrystalline material obeying the above condition scales as the sixth power of grain size.

Metglas 2826 MB is an alloy, with composition $Fe_{40}Ni_{38}Mo_4B_{18}$, possessing excellent soft magnetic properties, with a saturation magnetization of 87 emu g^{-1} [4]. The alloy is amorphous in nature and commercially available in the form of ribbons, with typical thickness of 20 μm and length of a few centimeters in length. The amorphous structure can be devitrified into a nanocrystalline state by thermal annealing or ion irradiation [5–7]. A nanocrystalline morphology is more favorable for superior soft magnetic properties since the microstructure of nanocrystals in an amorphous matrix can yield superior soft magnetic properties compared to their amorphous counterpart [8]. The combination of various physical properties resulting from nanocrystallization makes them ideal candidates for various sensor applications.

Various reports are available in literature regarding the kinetics of crystallization of $Fe_{40}Ni_{38}Mo_4B_{16}$ [6, 7, 9–11]. The enthalpy of formation and activation energy can be evaluated by employing various methods such as the Kissinger [12], Moyniham [13], and Marseglia [14] techniques. Fe-Ni-Mo-B follows a two-stage crystallization process [6, 7, 10]. The first stage is the Fe-Ni phase, which crystallizes by primary crystallization; the second phase is $(FeNiMo)_{23}B_6$, which crystallizes via polymorphic crystallization. The enthalpies of formation and activation energy for the two phases are 19.39 J g^{-1}, 3.49 eV $atom^{-1}$ and 54.09 J g^{-1}, 4.5 eV $atom^{-1}$, for Fe-Ni and $(FeNiMo)_{23}B_6$ phase respectively [6, 7, 10]. The as-prepared ribbons are amorphous and crystallization takes place with heat treatments. The Fe-Ni phase usually precipitates above 400 °C and $(FeNiMo)_{23}B_6$ above 500 °C [6, 7].

Since Metglas 2826 MB is widely used for sensor applications, integrating Metglas 2826 MB into MEMS/NEMS can add further functionality to these alloys. Metglas 2826 MB thin films find a variety of applications as magnetic sensors [15, 16], and as pinning layers in magnetic tunnel junctions and magnetic read heads. Attempts to fabricate thin film forms of Metglas 2826 MB were reported earlier by many researchers [17, 18]. For example, Jyothi *et al* used a flash evaporation technique whereas Liang *et al* used sputtering. Jyothi *et al* did not carry out composition analysis; they found that the deposited films were crystalline. Senoy *et al* and Hysen *et al* reported the fabrication of thin films from composite targets using vacuum evaporation [19, 20]. They also studied annealing and swift heavy ion irradiation effects on

these films and reported the formation of Fe-Ni nanocrystals with annealing [21, 22]. These nanocrystalline structures precipitate after annealing at 400 °C. However, they could not retain the stoichiometry of the original target in films owing to the variations in the vapour pressure of the different alloying elements in the target during the physical vapour deposition process. Annealing the films resulted in the precipitation of only the magnetic Fe-Ni phase, while annealing the ribbon resulted in the precipitation of both the ferromagnetic Fe-Ni phase and paramagnetic $(FeNiMo)_{23}B_6$. The mismatch in composition of target and film could be avoided by using techniques like RF sputtering or pulsed laser deposition. Retention of the stoichiometry of the target in thin film form is of the great interest as the stoichiometry of films can affect the structure and kinetics of phase transformation and its magnetic properties.

In this manuscript we report the fabrication of Fe-Ni-Mo-B thin films by RF sputtering and the evolution of their microstructure and magnetic properties with thermal annealing.

2. Experimental methods

2.1. Preparation of Fe-Ni alloy based thin films

The bulk Fe-Ni-Mo-B ribbons, having a thickness of 20 μm, were severed into a 2-inch diameter circle, which was subsequently used as the cathode for RF sputtering. The target was sputtered to silicon substrates. The silicon substrates were cleaned in three steps using trichloroethylene, acetone and isopropyl alcohol. The deposition was carried out with RF power of 100 watts for 30 min in argon atmosphere. Base pressure of 9×10^{-5} Torr was attained using a turbo pump backed by a scroll pump which elevated to 6×10^{-2} Torr during deposition. The as-deposited films were vacuum annealed for 1 h at temperatures of 400 °C and 600 °C. The film thickness was estimated from x-ray reflectivity (XRR) measurements carried out using a Bruker Discover D-8 with CuKα ($\lambda = 1.5406$ Å) radiation. The experimental data was fitted employing Parratt software [23].

2.2. Structural characterization

The structural characterization of pristine and annealed films were investigated using a Bruker Discover D-8 glancing angle x-ray diffractometer (GXRD) with CuKα ($\lambda = 1.5406$ Å) radiation. The measurement was carried out at grazing incidence of 0.5° and in the range 40° to 55° at a scan speed of 0.5° per minute. The crystallite size was calculated using the Scherrer formula $D = \dfrac{0.9\lambda}{\beta \cos\theta}$, where D is the crystallite size, λ the wavelength of x-rays, β the full width at half maximum in radians, and 2θ the diffraction angle. The micro-structural characterizations were performed using a tunneling electron microscope (TEM) (FEI F20) operated at 200 kV.

2.3. Compositional analysis

The composition of the films was investigated using x-ray photoelectron spectroscopy (XPS). Al K_α radiation having energy of 1486.6 eV was used as the source for XPS. The obtained XPS spectra were quantified using the Casa XPS program (Casa Software Ltd, USA).

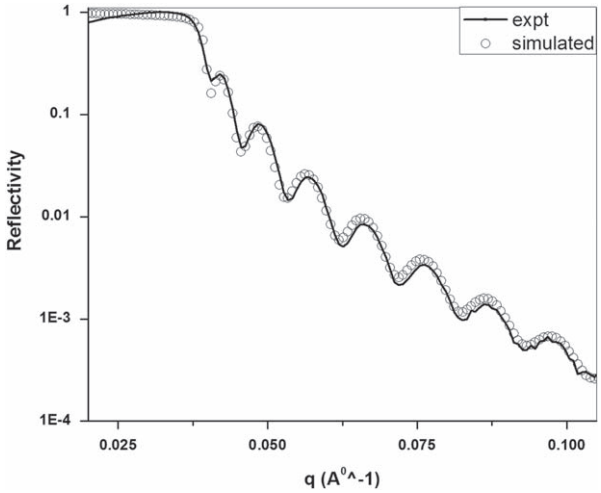

Figure 1. XRR image of pristine film.

2.4. Surface morphological studies

Surface morphological studies were carried out with an atomic force microscope (AFM) digital instruments nanoscope. The analysis of AFM images was done using the software Nanoscope 7.2 (Veeco Scientific Ltd).

2.5. Magnetic measurements

7 Tesla MPMS super-conducting quantum interferometer device (SQUID)—vibrating sample magnetometer (VSM) was employed to measure the magnetic properties. Room temperature magnetization measurements were carried out for magnetic fields −5 kOe to +5 kOe. Field-cooled and zero–field-cooled measurements were performed in the range of 10 K to 300 K and the field applied for field-cooled measurements was 200 Oe.

3. Results and discussion

3.1. XRR studies

The thickness of the films obtained by fitting the XRR data using PARRATT 1.6 software was found to be ∼52 nm (figure 1). No change in film thickness was observed with annealing.

3.2. Structural analysis

The GXRD results of the films are shown in figure 2. Contrary to the bulk ribbons [7, 9], the as-deposited film was crystalline in nature.

From the diffraction pattern we observe the films to be crystalline in nature. Since the Fe-Ni and $(FeNiMo)_{23}B_6$ phases have overlapping planes, it is difficult to conclude the phase from GXRD. To ascertain the precipitated crystalline phase, selected area electron diffraction (SAED) was carried out on the samples. Annealing the films did not change the peak position. The crystallite size calculated from the Sherrer formula was found to be 35.3 nm, 33.2 nm, and 35.9 nm for pristine and samples annealed at 400 °C and 600 °C, respectively. It was observed

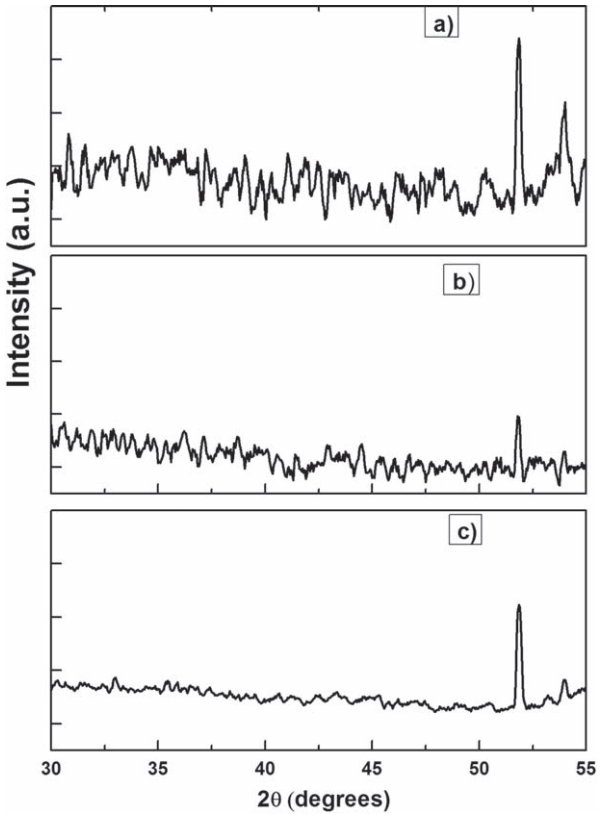

Figure 2. GXRD of (a) pristine film and film annealed at (b) 400 °C and (c) 600 °C.

that there was no significant change in the crystallite size with annealing. Ramanujan *et al* [10]. reported the effect of molybdenum on the crystallization of FeNiMoB ribbons. They observed that Mo inhibits the crystal growth by accumulating at the interface of Fe-Ni crystallites [10]. The pristine film itself is crystalline and we have observed that on annealing, no new phases are precipitated and that Mo might have inhibited further grain growth.

TEM of the pristine and film annealed at 600 °C is shown in figure 3. From TEM micrographs it is clear that the films are crystalline in nature, which is in agreement with GXRD results. The grain size of the films was found to be 10.8 nm and 11.6 nm for pristine and film annealed at 600 °C, respectively. The difference in grain size obtained from GXRD and TEM is due to the limitation of the Scherrer formula. The SAED images (figure 4) show well-defined rings signifying the polycrystalline nature of the film. The rings were indexed and they were compared with the standard data. The interplanar spacing for the pristine film was 2.46 Å, 2.01 Å and 1.45 Å, which corresponds to (420) plane of $(FeNiMo)_{23}B_6$ [ICDD No: 380888], (111) plane of Fe-Ni [ICDD No: 471417] and (440) plane of $Fe_{2.92}O_4$ [ICDD No: 861362], respectively. For the film annealed at 600 °C the *d* values are 1.98 Å, 1.68 Å and 1.20 Å, which corresponds to (200) plane of Fe-Ni, [ICDD No: 471417], (620) plane of $(FeNiMo)_{23}B_6$ [ICDD No: 380888] and (444) plane of $Fe_{2.92}O_4$ [ICDD No: 861362], respectively. From GXRD and SAED we conclude that the films are crystalline in nature. On sputtering, both Fe-Ni phase and $(FeNiMo)_{23}B_6$ phases are formed. From the available literature, the activation energy required for the precipitation of $(FeNiMo)_{23}B_6$ phase is larger than that required for the Fe-Ni phase [6, 7]. The RF power of 100 W must be sufficient for the formation of $(FeNiMo)_{23}B_6$ phase.

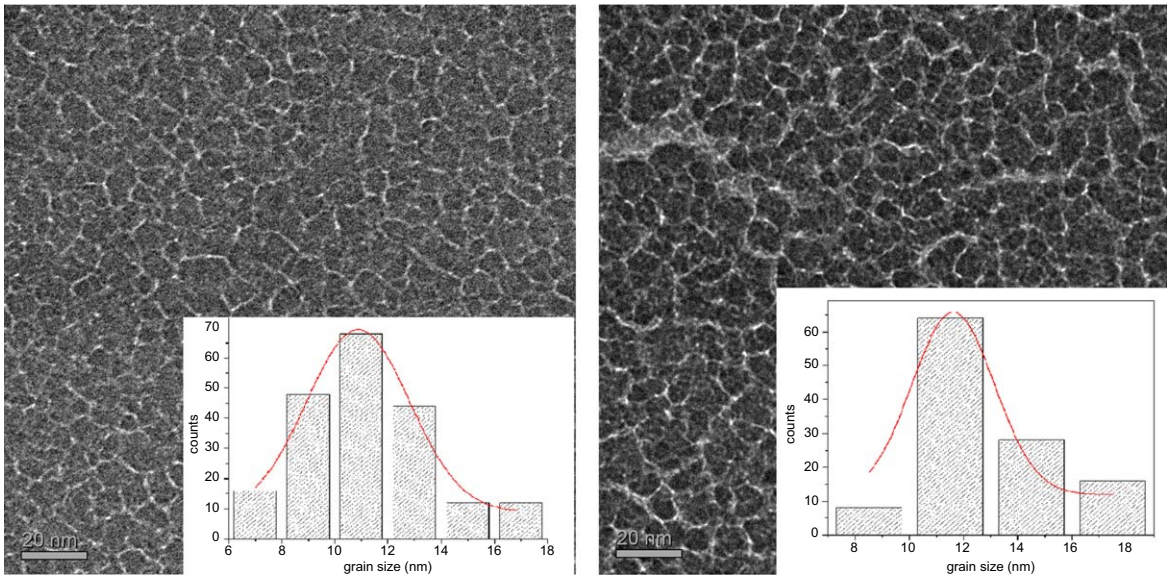

Figure 3. TEM micrographs and Crystallite size distribution (Inset) of pristine and film annealed at 600 °C.

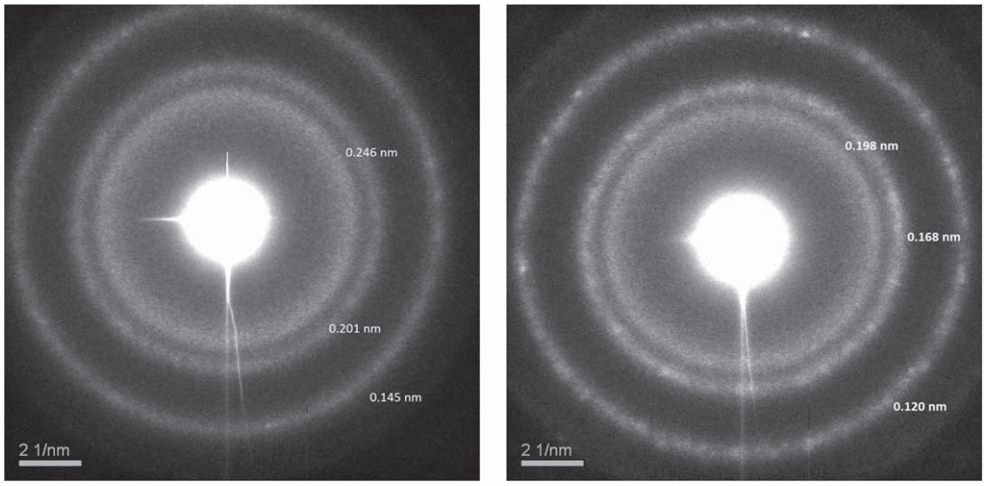

Figure 4. SAED of Pristine and film annealed at 600 °C.

Liang *et al* have reported magnetostrictive Metglas sensors by RF sputtering. They supplied an RF power of 30 W and reported Fe-Ni phase in thin films deposited at 10 mTorr [24, 18]. The RF power of 100 W results in the precipitation of both Fe-Ni and $(FeNiMo)_{23}B_6$ phases. Since Fe-Ni and $(FeNiMo)_{23}B_6$ have overlapping *d* values, it is difficult to ascertain the obtained phase. From the magnetic measurements discussed later, we have observed that the film exhibits very low saturation magnetization, which suggests that even though Fe-Ni phase is formed the predominant phase is $(FeNiMo)_{23}B_6$.

The crystallization kinetics for formation of the $(FeNiMo)_{23}B_6$ phase can be assumed as follows. Usually an amorphous solid can crystallize via primary crystallization, polymorphous crystallization, or eutectic crystallization. In primary crystallization the primary phase of the alloy crystallizes first. In polymorphous crystallization, there is a direct transition of the

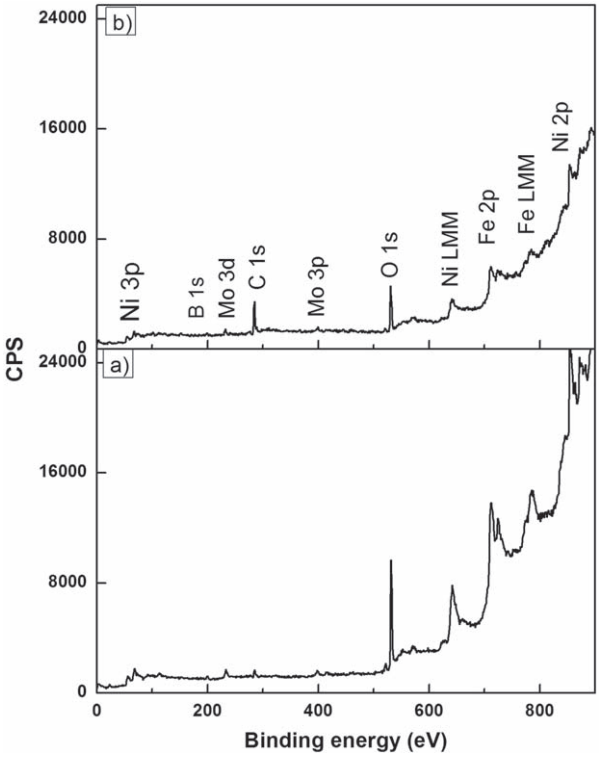

Figure 5. XPS of (a) pristine film and (b) film annealed at 600 °C.

amorphous phase to the crystalline phase [25]. In the present study, primary crystallization results in the precipitation of the Fe-Ni phase while the $(FeNiMo)_{23}B_6$ phase precipitates via polymorphous crystallization. However, further studies are required to confirm the crystallization kinetics of thin films.

3.3. Compositional analysis

The XPS of the samples is shown in figure 5. Since the film surface contains unavoidable oxygen and carbon, the XPS scan was carried out after sputtering the film surface for 30 min using 500 eV argon ions. From the XPS spectra it was possible to confirm the presence of Fe, Ni, Mo and B. XPS investigation was also carried out on the 600 °C annealed sample to investigate changes in surface composition with annealing. The composition of the pristine sample is 59.9% Fe, 25.9% Ni, 3.7% Mo and 10.3% B. For the sample annealed at 600 °C the composition is 36.4% Fe, 42% Ni, 11.5% Mo and 9.9% B.

We have succeeded in identifying boron and molybdenum in thin film samples and these elements play an important role in controlling the grain size and magnetic properties. Even after sputtering the film for 30 min, there is presence of carbon and oxygen. The presence of carbon and oxygen in the samples emanates from hydrocarbon contamination from the XPS unit. In the annealed sample, the carbon content has increased markedly while the iron content has decreased. Ciang *et al* reported that the presence of oxygen and carbon in the bulk was due to surface absorption while the presence of these in thin films was due to both absorption and deposition [24].

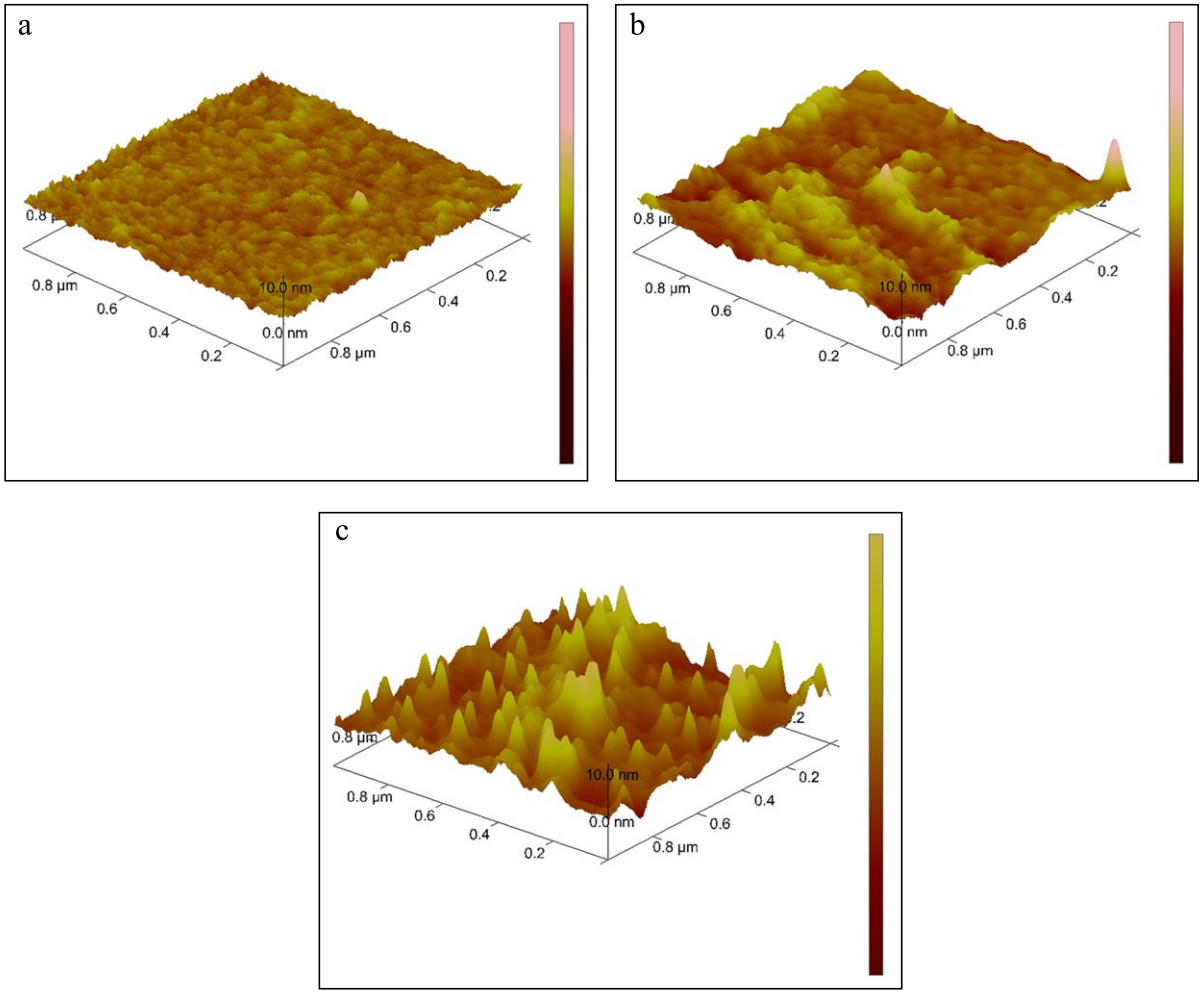

Figure 6. AFM images of (a) pristine and film annealed at (b) 400 °C and (c) 600 °C.

3.4. Surface analysis

The AFM images are shown in figure 6. The scan area was $1\,\mu\text{m} \times 1\,\mu\text{m}$. It is clear that significant surface evolution takes place with annealing. The variation of surface roughness is plotted in figure 7. From the AFM data, it can clearly be seen that the surface roughness increases with annealing temperature. RMS roughness (R_q) is a statistical parameter which gives the root mean square height of the film surface. However, it does not give any idea about the lateral distribution of surface features. This information can be obtained by power spectral density (PSD) analysis, which decomposes the surface profile into spatial spectral frequencies [25]. The PSD function is obtained by Fourier transformation of the surface and is given by $PSD(f) = \frac{1}{L^2}\left|\iint \frac{d^2r}{2\pi} e^{-if.r}\langle h(r)\rangle\right|^2$ [26]. The PSD spectra of the pristine and annealed films are shown in figure 8. The low-frequency region represents uncorrelated noise and the high-frequency region obeys a power law, $PSD(f) = Af^{-\xi}$, where ξ is the slope [27]. ξ for pristine film, and for films annealed at 400 °C and 600 °C are 1.6, 1.8 and 2.1, respectively. Herring and Mullins have reported the possible surface mechanism as plastic flow driven by surface tension,

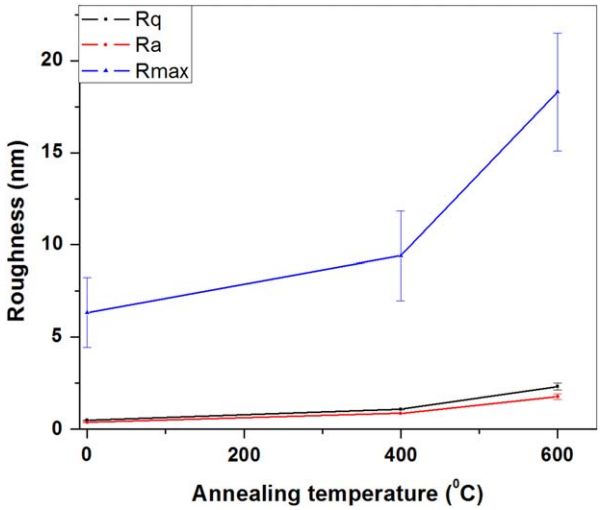

Figure 7. Variation of surface roughness with annealing temperature.

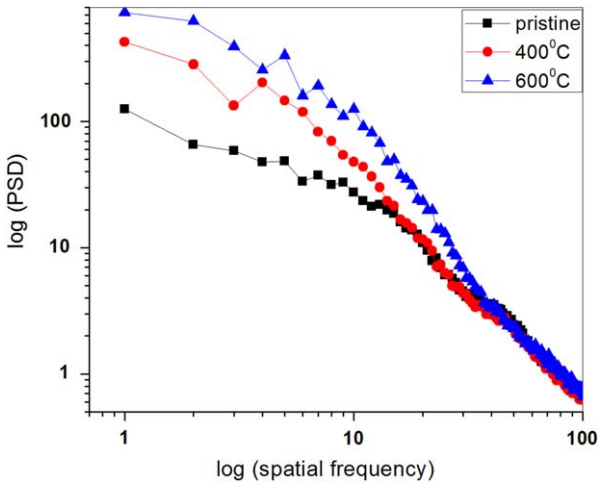

Figure 8. PSD spectra of pristine and film annealed at 400 °C and 600 °C.

evaporation condensation, volume diffusion and surface diffusion for ξ values 1, 2, 3 and 4 [21, 28, 29]. The ξ values increases on annealing. The possible surface mechanism in pristine and films annealed at 400 °C can be plastic flow driven by surface tension. For the films annealed at 600 °C, the increased roughness could be due to oriented grain growth as a result of annealing.

3.5. Magnetic studies

The M–H hysteresis loops of the pristine as well as the annealed samples were recorded at room temperature (figure 9). The changes in saturation magnetization and coercivity are shown in figure 10.

Compared to the bulk FeNiMoB ribbons, the films show a low value of saturation magnetization. Hysen *et al* [19] have reported a saturation magnetization of 70 emu g^{-1} for annealed films of Fe-Ni. In this investigation we obtained a very low value of saturation

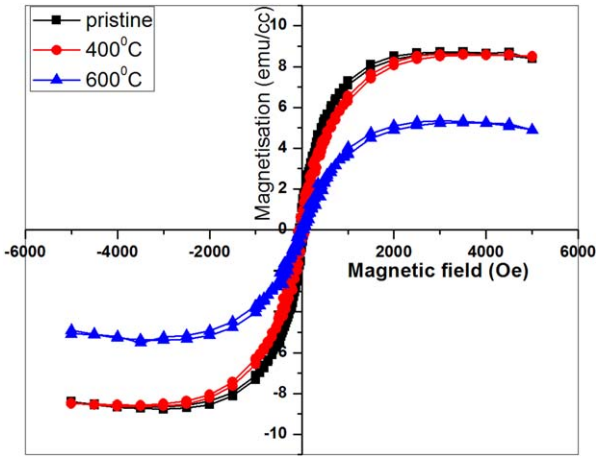

Figure 9. M–H measurements.

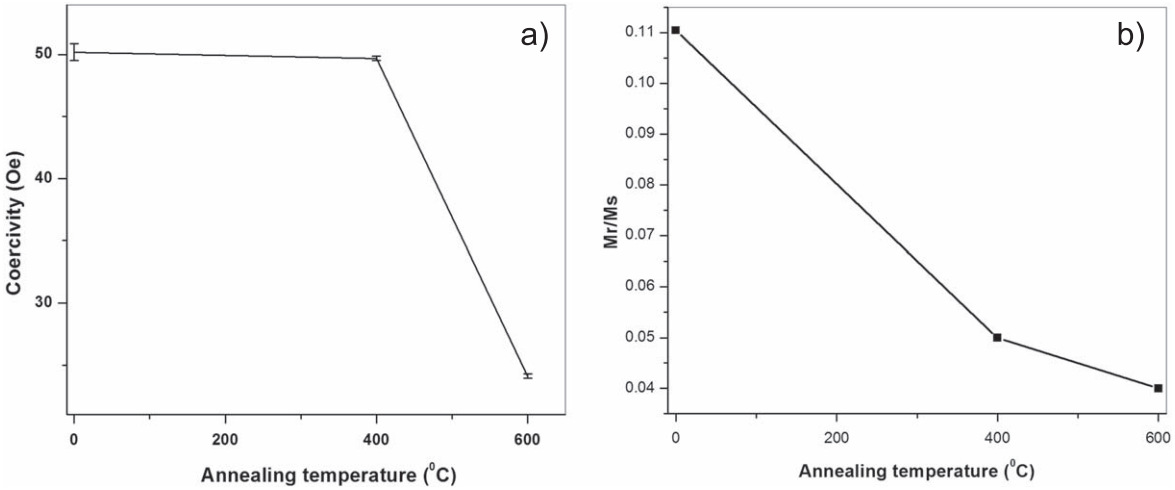

Figure 10. Variation of (a) coercivity and (b) M_r/M_s with annealing temperature.

magnetization for the annealed film. This is because of the presence of a predominant non-magnetic phase $(FeNiMo)_{23}B_6$, which is evident from GXRD and TEM analysis. There are reports of this non-magnetic phase by Ramanujan *et al* [6]. The small magnetization of films is due to the presence of a small fraction of the Fe-Ni phase. The film annealed at 600 °C exhibits very low saturation magnetization. The XPS results indicate that films annealed at 600 °C have a higher impurity content of carbon and oxygen. As a result of higher oxidation of the film, the saturation magnetization is further reduced. Earlier studies by Hysen *et al* [19] and Senoy *et al* [20] on the annealing effects of FeNiMoB thin films by thermal evaporation showed that Mo and B were not present in the film. The Fe Ni phase precipitated on annealing, resulting in a nanocrystalline structure exhibiting high saturation magnetization. Further, the magnetic properties exhibited by crystalline and amorphous materials are entirely different. FeNiMoB ribbons and thin films prepared by thermal evaporation are amorphous and good soft magnetic properties are reported. We have observed the film to be dominated by a nonmagnetic crystalline phase; thereby soft magnetic properties were found to be feeble [30].

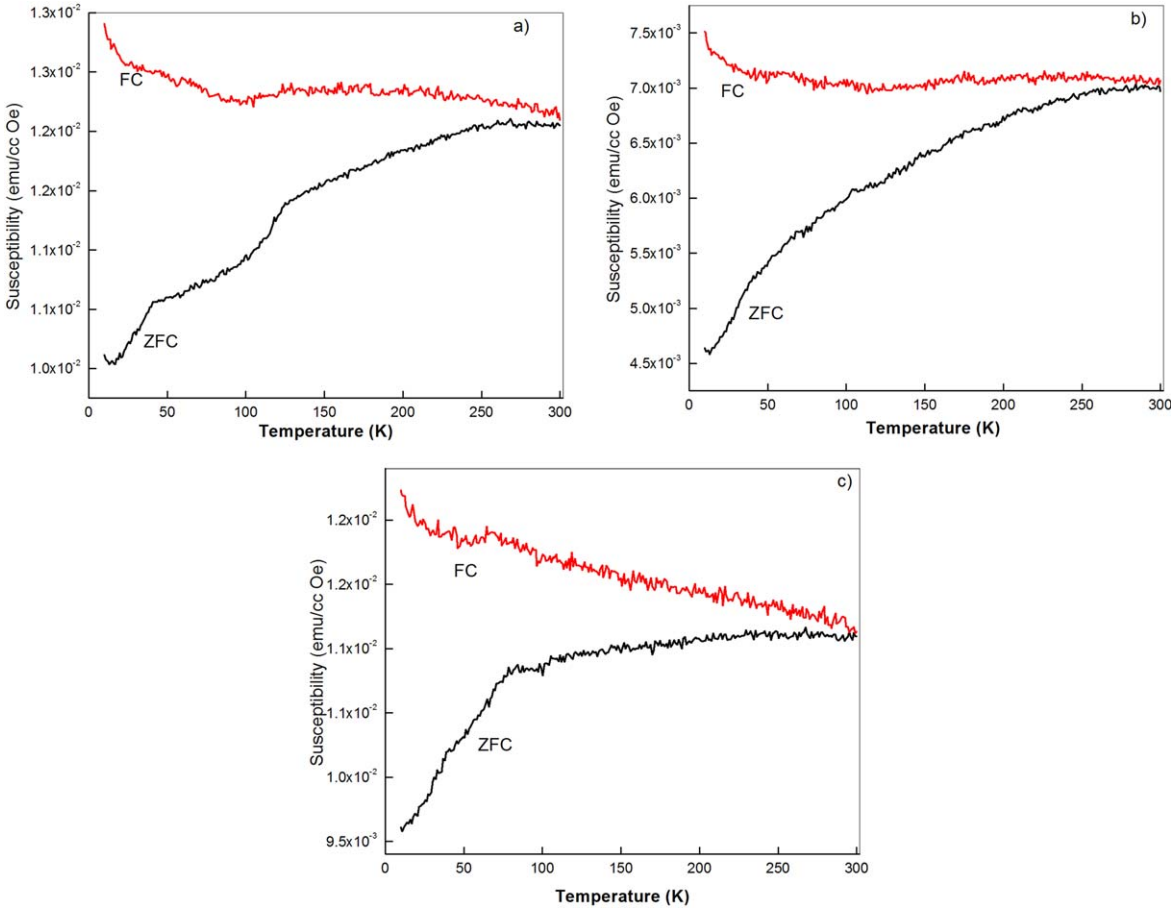

Figure 11. FC-ZFC studies of (a) pristine (b) film annealed at 400 °C and (c) 600 °C.

Field cooled and zero–field-cooled studies were conducted with a view to confirm the ferromagnetic behavior of the films. The results are shown in figure 11. The zero-field susceptibility increases with temperature, which is characteristic of a ferromagnetic material. T_{irr}, the temperature above where spin disorder takes place, was not observed until room temperature. This suggests that the material is ferromagnetic at room temperature and its Curie temperature is above 300 K. The small fraction of Fe-Ni phase contributes to the ferromagnetic behavior of the films.

4. Conclusions

Thin films of FeNiMoB were successfully prepared by RF sputtering. The thickness of the films obtained by XRR was ∼52 nm. The XPS studies have confirmed the presence of iron, nickel, boron and molybdenum in the thin film. The films were annealed at 400 °C and 600 °C. The pristine film was crystalline with the dominant phase being $(FeNiMo)_{23}B_6$. We obtained this phase by sputtering the target with an RF power of 100 watts. GXRD results indicate that molybdenum inhibited grain growth in the annealed films. The surface morphology of the film underwent changes with annealing. PSD analysis indicates plastic flow as the possible surface evolution mechanism in pristine film, while surface roughening due to oriented grain growth is

observed for the films annealed at 400 °C and 600 °C. All the films were soft magnetic in nature, exhibiting low coercivity. The films annealed at 600 °C show much smaller coercivity. However, we were not able to obtain high-saturation magnetization, as reported earlier. This is attributed to the formation of the $(FeNiMo)_{23}B_6$ phase. Further systematic study can be carried out on RF-sputtered thin films to establish the kinetics and phase formation.

Acknowledgement

LR and MRA are grateful to IUAC, New Delhi for providing financial assistance in the form of UFUP project. LR is thankful to a) V V Sivakumar, Scientist, IUAC for helping in the deposition of thin films by RF sputtering, b) Abhilash, Engineer at IUAC New Delhi, for his timely help in the target lab, c) Dr Ajay Gupta, Centre Director; Dr V Ganesan; Dr T Shripathi; Scientist H; Dr V R Reddy; Dr Ram Janay Choudhary, and Scientist E of UGC DAE CSR, Indore for carrying out characterizations and measurements, d) Dr Shilpa Tripathi, Research Associate, UGC DAE CSR Indore for help in XPS measurements, e) Mr Anil Gome, Junior Engineer and Mr Mohan Gangrade, Scientific Assistant, UGC DAE CSR, Indore for their help in doing XRR, GXRD, and AFM measurements, f) Ms Komal Bapna, Project Associate II, UGC DAE CSR Indore for her help in SQUID VSM measurements. MRA acknowledges the DST-DAAD project for funding. GP acknowledges UGC, India for providing financial assistance in the form of RFSMS fellowship (No.F4-3/2006(BSR)/8-3/2007(BSR)).

References

[1] Makino A, Hatanai T, Naitoh Y and Bitoh T 1997 *IEEE Trans. Magn.* **33** 3793
[2] Clement W, Willens R H and Duwez P 1960 *Nature* **187** 869
[3] Herzer G 2005 *J. Magn. Magn. Mat.* **294** 99
[4] Krishnan R, Prasad S and Branska K 1979 *J. Appl. Phys.* **50** 7639
[5] McHenry M E, Willard M A and Laughlin D E 1999 *Prog. Mater. Sci.* **44** 291
[6] Du S W and Ramanujan R V 2005 *J. Non-Cryst. Solids* **351** 3105
[7] Hysen T, Senoy T, Ramanujan R V and Anantharaman M R 2008 *J Mater. Sci.* **43** 635
[8] Herzer G 1990 *IEEE Trans. Magn.* **26** 1397
[9] Du S W and Ramanujan R V 2004 *Mater. Sci. Eng.* A **375** 1040
[10] Ramanujan R V and Du S W 2006 *J. Alloys Compd.* **425** 251
[11] He K-Y, Zhao Y-H, Li G-G, Cheng L-Z, Wu B, Sui M-L and Chen W-Z 2007 *J. Magn. Magn. Mat.* **316** 34
[12] Kissinger H E 1957 *Anal. Chem.* **29** 1702
[13] Moynihan C T, Easteal A J, Wilder J and Tucker J 1974 *J. Phys. Chem.* **78** 267
[14] Marseglia E A 1980 *J. Non-Cryst. Solids* **41** 31
[15] Thomas S, Mathew J, Radhakrishnan P, Nampoori V P N, George A K, Al Harthi S H, Ramanujam R V and Anantharaman M R 2010 *Sens. Actuators* A **161** 83
[16] Stoyanov P G and Grim C A 2000 *Sens. Actuators* **80** 8
[17] Jyothi M and Suryanarayana C 1985 *Z. Metallk.* **76** 802
[18] Liang C, Hu J, Prorok B, Gooneratne C and Kosel J 2011 *Mater. Sci. Forum* **667** 1207
[19] Hysen T, Deepa S, Saravanan S, Ramanujan R V, Avasthi D K, Joy P A, Kulkarni S D and Anantharaman M R 2006 *J. Phys. D: Appl. Phys.* **39** 1993
[20] Thomas S, Al-Harthi S H, Sakthikumar D, Al-Omari I A, Ramanujan R V, Yoshida Y and Anantharaman M R 2008 *J. Phys. D: Appl. Phys.* **41** 155009

[21] Thomas H, Thomas S, Ramanujan R V, Avasthi D K, Al-Omari I A, Al-Harthi S and Anantharaman M R 2012 *Nucl. Instrum. Methods Phys. Res., Sect.* B **287** 85
[22] Thomas S, Thomas H, Avasthi D K, Tripathi A, Ramanujan R V and Anantharaman M R 2009 *J. Appl. Phys.* **105** 033910
[23] Parratt L G 1954 *Phys. Rev.* **95** 359
[24] Liang C 2007 Development of bulk-scale and thin film magnetostrictive sensor *Dissertation* Auburn University pp 168–71
[25] Gavrila R, Dinescu A and Mardare D 2007 *Rom. J. Inf. Sci. Technol.* **10** 291
[26] Petri R, Brault P, Vatel O, Henry D, Andre E, Dumas P and Salvan F 1994 *J. Appl. Phys.* **75** 7498
[27] Dash P, Mallick P, Rath H, Tripathi A, Prakash J, Avasthi D K, Mazumder S, Varma S, Satyam P V and Mishra N C 2009 *Appl. Surf. Sci.* **256** 558
[28] Herring C 1950 *J. Appl. Phys.* **21** 301
[29] Mullins W W 1959 *J. Appl. Phys.* **30** 77
[30] Nozieres J P, Ghidini M, Dempsey N M, Gervais B, Givord D, Suran G and Coey J M D 1998 *Nucl. Instrum. Methods Phys. Res., Sect.* B **146** 250